Aeroacoustics Analysis of Radiator Installation Effects in a Pulling Engine Cooling Module

Proceedings

INTERNATIONAL CONFERENCE ON FAN NOISE, AERODYNAMICS, APPLICATIONS AND SYSTEMS

9 to 11 APRIL 2025
ANTIBES - JUAN-LES-PINS, FRANCE

Organized by

cetiat ensemble, innover et valider

CETIM

www.fan2025.org

Published by
Sigel Press
8187 Camp Road
Homerville, Ohio, USA

Visit us on the WorldWideWeb at: www.sigelpress.com

Internal Design: Professional Book Compositors, Lorain, Ohio, USA
Cover Design: Francois Bessac
Cover Images: Cetiat

ISBN 978-1-905941-32-2

Typeset in Times Roman

The publisher's to use paper manufactured from sustainable forests.

Proceedings of FAN 2025

8th International Conference on Fan Noise, Aerodynamics, Applications and Systems, 9 to 11 April 2025, Antibes, Juan-les-Pines, France.

1. Fan Noise 1992: Senlis, France, 1-3 September 1992.
2. Fan Noise 2003: Senlis, France, 23–25 September 2003.
3. Fan Noise 2007: Lyon, France, 17-19 September 2007.
4. Fan 2012: Senlis, France, 18-20 April 2022.
5. Fan 2015: Lyon, France, 15-17 April 2015.
6. Fan 2018: Darmstadt, Germany, 18-20 April 2018.
7. Fan 2022: Senlis, France, 27-29 June 2022.

Organizers

CETIAT
Centre Technique des Industries Aérauliques et Thermiques
Domaine Scientifique de la Doua,
25 avenue des Arts, BP 52042
69603 Villeurbanne Cedex - France
Phone: +33 472 44 49 00
E-mail: commercial@cetiat.fr
www.cetiat.fr

CETIM
Technical Centre for Mechanical Industries
52 Avenue Félix Louat, BP 80067
60304 Senlis - France
Phone: +33 (0)6 70 01 53 17
E-mail: marc-olivier.sinanian@cetim.fr www.
cetim-engineering.com

AEROACOUSTIC ANALYSIS OF RADIATOR INSTALLATION EFFECTS IN A PULLING ENGINE COOLING MODULE

Francesco BELLELLI[1], Renzo ARINA[1],
Stéphane MOREAU[2], Francesco AVALLONE[1]

[1]*Department of Mechanical and Aerospace Engineering, Politecnico di Torino, Corso Duca degli Abruzzi 24, Torino, 10129, Italy*

[2] *Department of Mechanical Engineering, Université de Sherbrooke, 2500 Boulevard de l'Université, Sherbrooke, QC, J1K1R1, Canada*

SUMMARY

Fan noise is a critical issue for manufacturers, as they must balance aerodynamic and acoustic performance. Coupling a fan with a radiator in a pulling configuration, introduces significant challenges. Since it is challenging to perform scale resolved simulations of a radiator, an equivalent fluid approach is adopted. This study investigates the effects of an equivalent porous medium mimicking the radiator, and casing geometry on inflow and noise sources in an industrial cooling fan. Three configurations (Fan + Frame + Equivalent Porous Medium, Fan + Frame, Fan) are investigated using high-fidelity simulations. While aerodynamic performance remains consistent, the equivalent porous medium and casing geometry introduce inflow distortions, causing tonal noise variations, particularly in the full module configuration.

INTRODUCTION

With the increasing demand for electric vehicles, the need for high-performance cooling fans has intensified, particularly to manage heat during fast charging cycles. In practical applications, fans are usually paired with radiators, which affects the cooling module aerodynamic and acoustic performance making a challenge their performance prediction.

Sortor [1] stressed the sensitivity of both aerodynamic and acoustic performance to the installation effects of the radiator; it is essential to account for this coupling when installing different fans on the same radiator geometry. Therefore, a detailed description of the interaction between the fan and the radiator is essential to improve the overall efficiency and reduce noise of these systems.

Literature reports a wide variety of experimental studies on the effects of radiator-induced turbulence on fan aeroacoustic performance. Wagner et al. [2] examined the effect of the axial spacing between radiator outlet and fan inlet, highlighting its impact on noise levels at the blade passing frequency (BPF) and harmonics. Czwielong et al. [3] demonstrated that reducing the diameter of coolant tubes,

when large compared to the fan-radiator spacing, reduces the broadband noise, while the shape of the casing affects the tonal component. They also demonstrated the noise-reduction benefits of circular casing shapes compared to rectangular ones, due to a smoother casing-to-fan shape transition in the former case. However, their radiator technology might not be representative of industrial state of the art. Zarri et al. [4] showed that the thin coolant tubes are responsible for breaking down the turbulent eddies and increasing the non-homogeneity of the turbulence, while the presence of an upstream casing contributes to slightly shift turbulence towards anisotropy. This last aspect, although widely experimentally assessed in terms of turbulent energy spectra, still lacks a detailed three-dimensional flow description. Such a description can be obtained through numerical simulations, providing further insights into the rotor-inflow interaction. However, most numerical studies on isolated fans assume a uniform pressure drop, which does not adequately capture the complexities introduced by the radiator, as emphasized by Zhang et al. [5]. By adopting a porous medium model, Tebib et al. [6] showed that modelling the radiator as an equivalent porous medium produces sufficiently accurate numerical predictions of the aeroacoustic performance of the fan for industrial applications, and that including the tubes have no significant acoustic effect. However, the specific impact of this non-uniformity on the aerodynamic and acoustic properties of the system remains unclear.

The purpose of this paper is to address the impact of considering an equivalent porous medium, as opposed to a uniform pressure drop, and the transition in shape from square to round between the radiator casing and the fan on the upstream aerodynamics and, subsequently, on the noise sources of a realistic engine cooling module where the radiator is placed upstream of the fan. For this purpose, scale-resolved high-fidelity numerical simulations are carried out with the lattice-Boltzmann method (LBM) by means of the commercial software PowerFLOW by 3DS. Reference experimental data, acquired and provided by the manufacturer, are used to validate the numerical simulations.

The first section briefly summarizes the reference geometry, while the second section presents the numerical setup used to perform simulations. The grid convergence study and the validation of the numerical simulations against the experiments are discussed in the third section. The fourth section discusses the results, while the main conclusions are reported in the fifth section.

FAN AND RADIATOR GEOMETRIES

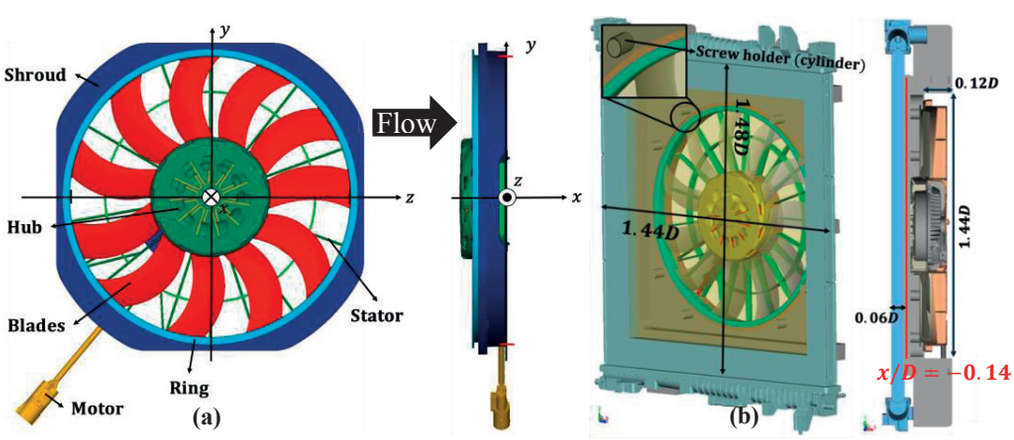

Figure 1: Tested engine cooling module parts. (a): Fan. (b): Radiator.

Fig. 1 shows the geometries of the fan and the radiator object of this study as well as the coordinate system that will be used to define the absolute position of planes and probes. The fan (Fig. 1a) consists of a 465 mm diameter (D) rotor with $B = 11$ unevenly spaced blades connected to a ring, a hub, a driving electrical motor, $V = 20$ unevenly spaced stator vanes, and a shroud. The fan tip clearance is equal to $0.009\ D$. The radiator (Fig. 1b) consists of a $1.48\ D \times 1.44\ D$ core placed $0.02\ D$ upstream of the fan hub and of a square casing that joins it to the fan through

FAN 2025
Antibes Juan-les-Pins (France), 9 – 11 April 2025

8 screws, covered by upstream protruding cylinders. The light blue solid part of the core joint with the square casing in grey will be referred as "Frame" in the rest of the paper.

Volume flow rate, torque and fan rotational speed are measured in an aerodynamic facility, while sound pressure level measurements are performed in a semi-anechoic room, in which the fan is placed at a distance $z/D = 3.23$ from the floor and a microphone is placed $2.15D$ upstream of the fan, aligned with its rotational axis. The module is described using non-dimensional parameters as it is an industrial product. Aerodynamic measurements are carried out along the full operating range for both the fan only and the complete cooling module, while acoustic measurements are carried out only at free blowing conditions for the complete cooling module, corresponding to load coefficient equal to $\psi = \frac{\text{pfs}}{\frac{1}{2}\rho v_{tip}^2} = 0$ and flow coefficient equal to $\varphi = \frac{qV}{\pi\left(R_{tip}^2 - R_{hub}^2\right)v_{tip}} = 0.13$, where pfs is the pressure rise through the cooling module, v_{tip} is the tip velocity, and qV is the volume flow rate through the fan. In both the air performance and acoustic measurements, the fan rotational speed is equal to $n = 3048\ rpm$.

NUMERICAL SETUP

The CAD geometries were provided by the. Three configurations are analysed: (i) the full cooling module (Fan + Frame + Porous Medium), (ii) the Fan + Frame, and (iii) the Fan.

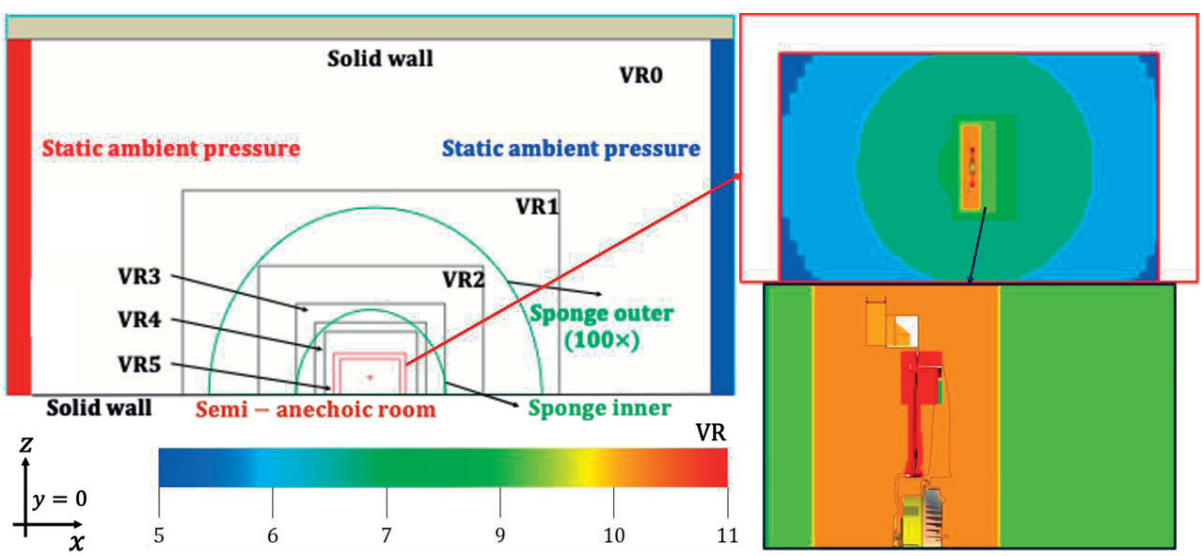

Figure 2: Sketch of the computational domain in the plane at $y/D = 0$.

The computational domain used to simulate all the configurations is shown in Fig. 2. The same numerical simulation setup was previously validated by Bellelli et al. [7]. A large fluid domain of $135\ D \times 135\ D \times 135\ D$ is built enclosing the semi-anechoic room. The room walls, of the same size as the experimental one, are modelled as an equivalent porous medium with viscous resistance equal to $50000\ 1/s$. The floor is modelled as a solid reflective wall. A discretization strategy, based on 11 Variable Resolution (VR) regions, is adopted. The regions with maximum resolution are set around the rotating blades and near the tip gap region, where for the most refined case there are 11 voxels in the tip clearance. In the VR3 region, a sponge region is defined by an artificial change of viscosity by a factor of 100 with an exponential function between the regions marked as “Sponge inner” and “Sponge outer” in Fig. 2. Inlet and outlet have a boundary condition equal to the static ambient pressure. In the full module configuration, the radiator is modelled as an equivalent porous medium [8]. In the Fan + Frame and Fan configurations, as the equivalent porous medium is removed, the fan is provided with a pressure rise that matches the pressure loss of the equivalent porous medium at the

same operating condition. To impose the matching pressure rise, a thin and acoustically absorbing wall, mimicking a wind tunnel aerodynamic facility is added. The pressure rise is imposed by initializing the flow on the suction side of the domain with a static pressure equal to the difference between the ambient pressure and the pressure rise. The inlet boundary condition is changed accordingly.

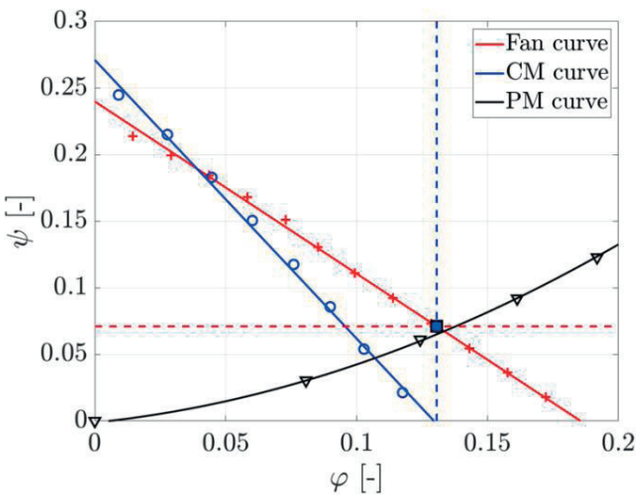

Figure 3: Experimental curves of fan alone (Fan), complete cooling module (CM), and radiator alone (PM).

The experimental aerodynamic curves of the complete module, fan alone, and radiator are shown in Fig. 3. The matching pressure rise is calculated as the pressure rise that the fan achieves at the same flow rate as the one at free discharge ($\psi = 0$) of the complete module i.e. $\varphi = 0.13$. A matching pressure rise of $\psi = 0.071$ is obtained. It is worth noting that the radiator pressure loss matches the pressure rise at $\varphi = 0.13$, resulting in almost no installation effect on the complete module.

60 revolutions are simulated for every case and time-averaged values are obtained by averaging over the last 10 revolutions. Simulations have been performed at three different resolutions of 300, 600, and 1200 voxels per diameter (vox/D) in the finest VR region. Far-field noise spectra are calculated using the Welch [9] averaging algorithm with 50% overlap and 8 Hamming windows directly from the simulation data, with a frequency resolution of 11.8 Hz and a sampling frequency of 48,000 Hz.

GRID CONVERGENCE STUDY

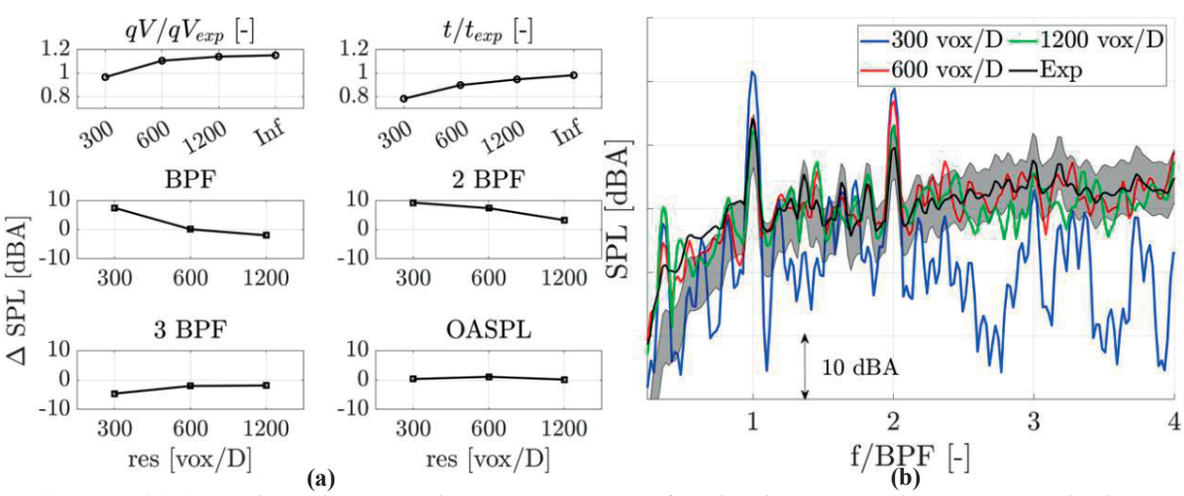

Figure 4. (a): Integral aerodynamic and acoustic quantities referred to the corresponding experimental values. (b): Sound Pressure Level in dBA obtained at x/D=-2.15 upstream of the fan (aligned with the fan rotation axis). The solid black line is the averaged experimental signal, while the grey shade is the variation in SPL each 10 revolutions.

The volume flow rate through the fan and aerodynamic torque obtained from the simulation of the complete cooling module configuration are shown in Fig. 4a made dimensionless by the corresponding experimental values. The "Inf" values are obtained through a Richardson extrapolation [10] with refinement ratio $r = 2$ and order of convergence $p = 2$ [11]. The figure shows that grid convergence is reached for the finest resolution case, as the extrapolated values are within 2% of the finest resolution. The volume flow rate exhibits a more evident convergence, although resulting in a slight overestimate of the experimental value. On the other hand, the torque is characterized by a steeper variation between resolutions and underestimates the corresponding experimental value. The differences in torque can be due to the difficulty in measuring a pure aerodynamic torque, while the differences in flow rate might be associated with the presence of complex flow phenomena in the casing as well, as shown by Moreau et al. [12]. These results are aligned with similar cases in the literature [13]. In addition, Fig. 4a shows the Sound Pressure Level (SPL) at the BPF and the first two harmonics as well as the Overall Sound Pressure Level (OASPL) in terms of discrepancies against the experimental values. Increasing the resolution the difference with respect to the experimental values is within 3 dB. In particular, the BPF and first harmonic are overestimated, while the second harmonic is underestimated; the OSPL instead shows drastically less sensitivity to the resolution.

To further investigate the impact of the grid resolution on far-field noise, the noise spectrum obtained with a direct probe at $x/D = -2.15, y/D = z/D = 0$ upstream of the fan at the three grid resolutions is compared against the experimental one in Fig. 4b. The probe is located $1.93D$ upstream of the radiator and is aligned with the fan rotation axis. A grey-shaded area has been superimposed on the plot, representing the variation in the SPL during the entire sampling time of the experimental values ($30\ s$) considering time-windows of 10 revolutions, i.e. the same number of revolutions sampled in the numerical simulations. One can note that the coarse resolution of $300\ vox/D$ is not sufficient to properly capture the broadband content, while the tones up to the first BPF harmonic are overestimated; this justifies why the OASPL is not different from the experiments. The medium ($600\ vox/D$) and fine ($1200\ vox/D$) resolutions are instead able to correctly predict the broadband levels and are characterized by a less prominent tonal content at BPF and harmonics. The $1200\ vox/D$ resolution shows better agreement at higher BPF harmonics; therefore, the results in the rest of this paper are shown only for the finest resolution.

RESULTS AND DISCUSSION

Table 1: Averaged aerodynamic integral quantities percentage variations with respect to the full cooling module configuration (Fan + Frame + PM). For each case, the quantities have been averaged over the last 10 revolutions.

	Fan + Frame + PM	**Fan + Frame**	**Fan**
ΔF	-	-14%	-5%
ΔqV	-	+2%	+1%
Δt	-	-5%	-6%

First, the impact of the different configurations on the overall aerodynamic performances is assessed. In Tab. 1 the average axial thrust force (F), volume flow rate through the fan (qV), and aerodynamic torque (t) are shown as percentage variations (Δ) with respect to the full cooling module configuration. Removing the equivalent porous medium (Fan + Frame) has a significant effect both on thrust and torque, which are reduced respectively by 14% and 5%, while keeping the flow rate mainly unaltered. It is also observed a similar trend in the torque and the volume flow rate when the Fan alone configuration is considered. However, it is interesting to note that the thrust has a lower decrease in this configuration rather than in the intermediate Fan + Frame configuration. The differences in the thrust and torque can be explained by looking at the different pressure patterns upstream of the fan.

FAN 2025
Antibes Juan-les-Pins (France), 9 – 11 April 2025

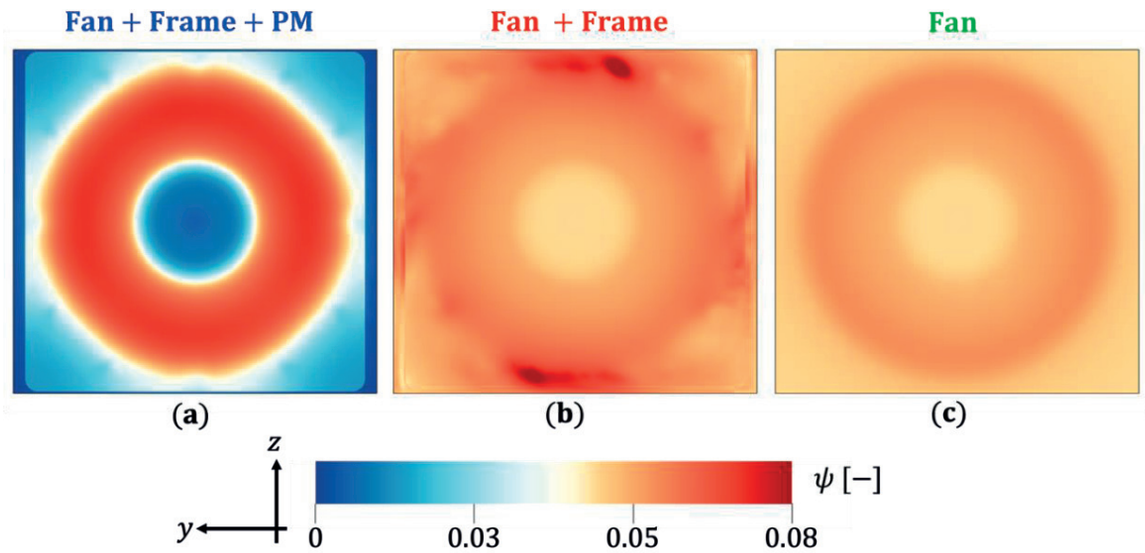

Figure 5: Mean pressure loss with respect to the ambient pressure in a plane located at x/D=-0.14, upstream of the fan. (a): Fan + Frame + PM. (b): Fan + Frame. (c): Fan.

In Fig. 5 the contour of the pressure rise with respect to the ambient pressure for all the simulated configurations in a plane located at $x/D = -0.14$ (see Fig. 1 for the plane location) are shown. The effect of the equivalent porous medium (Fig. 5a) is evident, as it concentrates the pressure loss mainly on the fan disk, unlike the Fan + Frame (Fig. 5b) and Fan (Fig. 5c) configurations, that show a more uniform distribution of ψ. This behavior is a direct consequence of the fact that the equivalent porous medium gives a pressure loss that depends on the inflow velocity. Therefore, it will result in higher pressure losses just on the region characterized by higher inflow velocities, such as the fan disk. Then, it can be noted that the square casing (Fig. 5b) is responsible for high ψ spots in the middle of each side. They can be attributed to the flow distortions caused by the square-to-round shape transition between the casing and the fan, that causes local stronger flow acceleration in the regions of shorter fan-frame distance. Finally, the Fan alone configuration (Fig. 5c) is characterized by a highly uniform distribution of ψ as the equivalent porous medium is removed, as well as any possible source of flow recirculation and inflow distortion.

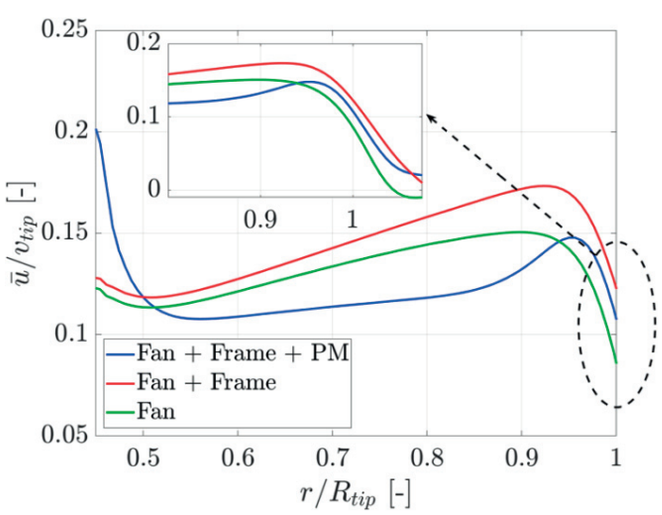

Figure 6: Mean axial velocity profile, azimuthally averaged, at x/D=-0.14. A zoom in the near tip region is shown in the top of the figure.

The azimuthally averaged axial velocity made dimensionless using v_{tip} at $x/D = -0.14$ is shown in Fig. 6. The full cooling module configuration shows the lowest values of $\bar{u}/v_{tip}$ for

$0.5 \leq r/R_{tip} \leq 0.95$ because of the greater pressure losses seen in Fig. 5. On the contrary, near the hub, at $r/R_{tip} \leq 0.5$, $\bar{u}/v_{tip}$ is the highest, as ψ is nearly equal to zero. Moreover, an increase in the axial velocity gradient for $0.9 \leq r/R_{tip} \leq 1$ is seen in the top of Fig. 6 because of the non-uniform ψ seen in Fig. 5. The Fan + Frame configuration shows a $\bar{u}/v_{tip}$increase for $0.7 \leq r/R_{tip} \leq 0.95$ due to the flow distortions seen in Fig. 5 while negligible differences in the near tip region are seen.

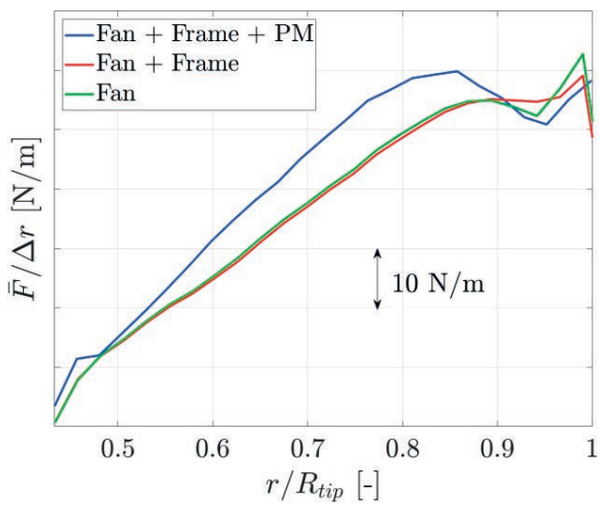

Figure 7: Mean thrust per unit length distribution on one blade, averaged on the last 10 revolutions.

The radial distribution of thrust per unit length is shown in Fig. 7. The full cooling module configuration is characterized by higher thrust per unit length up to $r/R_{tip} \leq 0.9$ due to higher ψ on the fan disk. The velocity decrease near the tip, seen in Fig. 6, results in lower thrust per unit length values for $r/R_{tip} \geq 0.9$. Moreover, the different flow topologies in the hub, shown in Fig. 6, is causing the thrust per unit length to experience a slight hump near $r/R_{tip} = 0.45$, which is also associated with flow recirculation in the hub. It is worth mentioning that the hub has several small slots to allow cooling of the driving electric motor; therefore, flow recirculation is present in those areas, especially in the presence of strong gradients such as when the equivalent porous medium is present. Finally, the effect of the frame is seen to be mainly located at the tip, where the distribution shows a higher drop. This is related to the presence of flow recirculation in the casing.

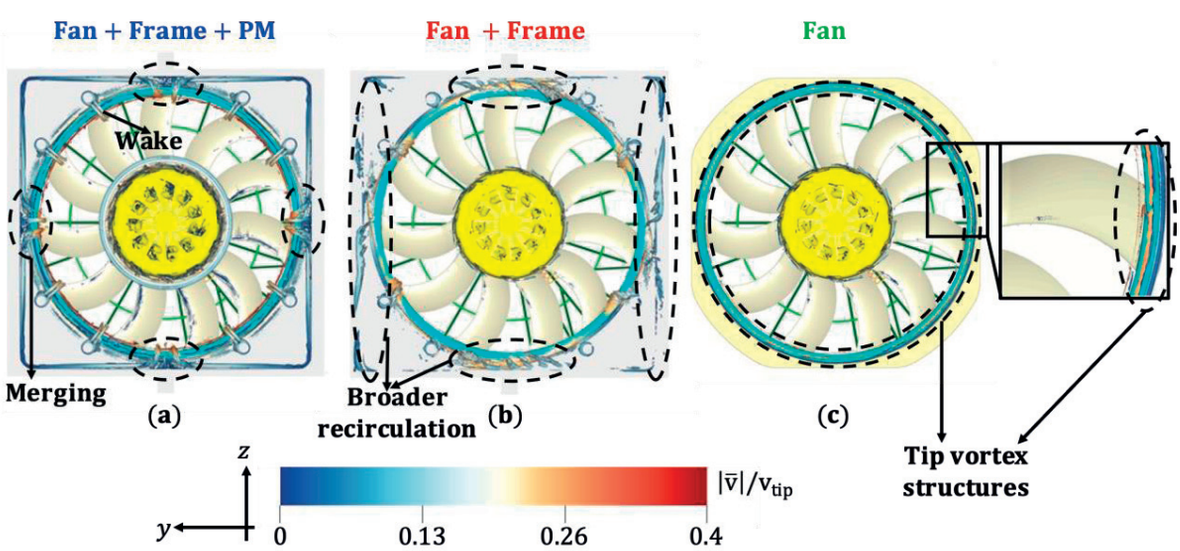

Figure 8: Mean $\Lambda_2 = -2.5 \cdot 10^5\ 1/s$ iso-surfaces coloured with velocity magnitude, in the casing upstream.

FAN 2025
Antibes Juan-les-Pins (France), 9 – 11 April 2025

The above analyses have highlighted the relevant role of the flow recirculation in the casing on the mean flow topology and on the blade loading distribution. Therefore, the $\Lambda_2 = -2.5 \cdot 10^5\ 1/s$ iso-surfaces coloured with the non-dimensional velocity magnitude are shown in Fig. 8. This quantity is obtained after averaging the flow field over the last 10 revolutions to identify only the coherent vortex structures that are steady in time. Only the coherent structures in the square casing area are shown. First, one can note that the full cooling module configuration (Fig. 8a) is characterized by almost steady coherent vortex structures along the four sides of the casing which strongly merge at the centre of each side. Moreover, wakes are shed by the 8 cylinders that house the fixing screws, which are then ingested by the fan in the tip region. The Fan + Frame configuration (Fig. 8b) is characterized by a broader recirculation, with less coherent steady vortex structures, because of the less strong velocity gradients. The vortex structures that are present in this case can be caused by the flow distortions due to the square-to-round shape transition between the casing and the fan. Finally, the Fan configuration (Fig. 8c) shows very small steady vortex structures only localized in the near tip region, wrapping around the rotating ring, which can be associated with tip leakage flow phenomena. In this case, these structures are not well visible because they are highly unsteady, and they are averaged out. The different vortex structures topology seen in Fig. 8 is expected to drastically influence the loading fluctuations of the blades, as the rotor will interact with a highly non-uniform flow field upstream in the configurations with the solid frame at certain azimuthal locations.

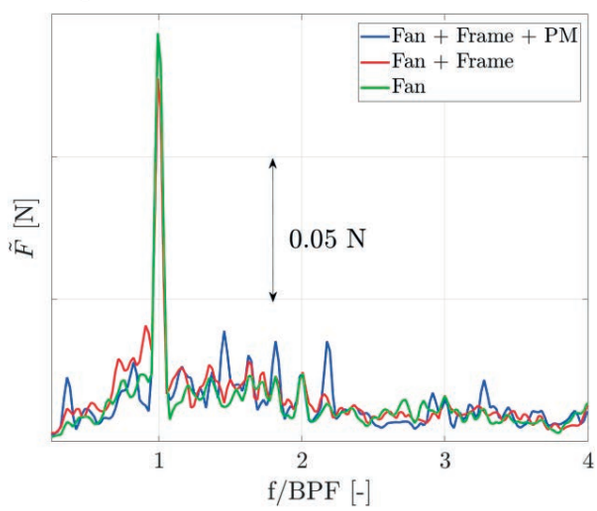

Figure 9: Spectra of the thrust given by all the 11 blades for the three configurations.

The spectral content of the unsteady thrust is shown in Fig. 9. The frequency axis is made dimensionless with respect to the BPF. The peak at the BPF is prominent in all the cases, with the Fan configuration showing the highest amplitude while the Fan + Frame configuration the lowest one. Furthermore, all the configurations show similar values at higher BPF harmonics. The cooling module configuration is characterized by several inter-harmonic narrow-band humps due to the periodic interaction of the blades with the vortices at the centre of each side of the casing and the wake of the 8 cylinders that hold the fixing screws. The Fan + Frame configuration is characterized by higher fluctuations for $0.5 < f/BPF < 1$ due to the stronger recirculation in the casing in this configuration. In contrast, the Fan alone case shows almost no inter-harmonic hump, except for a slight fluctuation at $f/BPF = 1.81$, which is associated with rotor-stator interaction phenomena, as both the blades and vanes are not equally spaced [10]. The blade loading fluctuations are subsequently expected to drive the acoustic footprint of the system, as typical in low-speed fan applications.

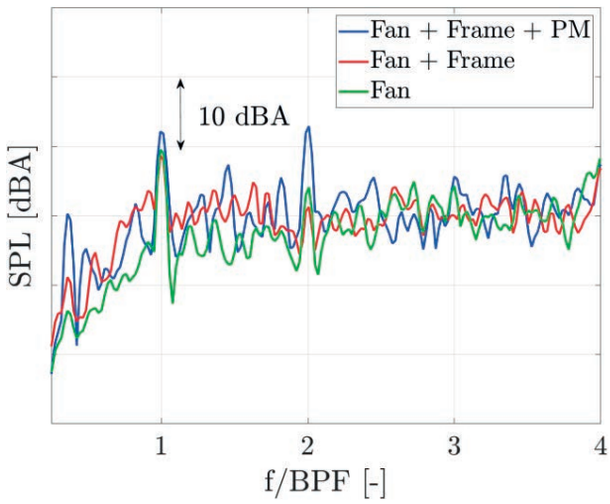

Figure 10: Far-field noise spectra at x=-2.15D upstream, along the fan axis.

Fig. 10 shows the spectra for the three configurations of the pressure fluctuations sampled at $x/D = -2.15$, $y/D = 0$, and $z/D = 0$, which corresponds to the upstream location on the fan axis. At the BPF and harmonics, the cooling module configuration is seen to have higher SPL. This can be associated both with the higher mean loading of this configuration, as shown in Fig. 7, and with the presence of recirculation in the semi-anechoic room, as pointed out in Refs. [7], [14], [15]. Furthermore, several inter-harmonic humps at frequencies $f/BPF = 4/11$ and harmonics are found. They are caused by the interaction between the rotor and the periodic inflow inhomogeneities due to the presence of the square casing and the 8 cylinders that house the screws, similarly to what is seen in Fig. 9. The broadband content of the spectra is characterized by a higher contribution of the Fan + Frame configuration at low and mid frequencies (approximately for $f/BPF < 2$), which can be attributed to the stronger recirculation pattern in the casing, as seen in Fig.5. The Fan configuration is then characterized by the absence of any inter-harmonic hump, as its inflow distribution is mostly uniform. Finally, the higher frequency broadband contribution (approximately for $f/BPF > 2$) shows almost the same levels for all four simulated configurations.

CONCLUSIONS

The impact of the radiator installation on the aerodynamic and aeroacoustics performance of a fan are analysed numerically considering three configurations: the full cooling module, where the radiator is replaced by an equivalent porous medium, the module without an equivalent porous medium but with the solid frame, and the fan alone. Simulations were performed at free blowing conditions. The latter two configurations have the same global pressure loss induced by the equivalent porous medium in the first configuration. Each of these factors plays a distinct role in modifying the fan performance and noise generation, particularly through their influence on upstream aerodynamics.

Removing the equivalent porous medium while maintaining the same pressure drop across the system results in a decrease in thrust and torque, slightly improving the aerodynamic efficiency. Moreover, the equivalent porous medium focuses the pressure losses on the fan disk, contributing to higher sectional blade loading in the axial direction. Removing the equivalent porous medium, pressure losses become more uniformly distributed across the system, affecting the distribution of aerodynamic loading along the blade and, therefore, the tonal noise of the fan at the BPF and harmonics. The increased inhomogeneity in the upstream flow amplifies the noise generated by interactions between the blades and the inflow distortions caused by the shape transition in the frame, particularly in the low frequency range. Furthermore, several inter-harmonic humps are present as a consequence of additional inflow distortions given by small cylindrical screw housings.

BIBLIOGRAPHY

[1] M. Sortor, «On-System Engine Cooling Fan Measurement as a Tool for Optimizing Cooling System Airflow Performance and Noise», *SAE Int. J. Mater. Manuf.*, vol. 4, fasc. 1, pp. 1221–1230, apr. **2011**, doi: 10.4271/2011-01-1169.

[2] S. Wagner e J. Rohlfing, «Effects of the fan - radiator interaction on the noise emissions of heat pumps: experimental and numerical studies», FAN2022, **2022**.

[3] F. Czwielong, J. Soldat, e S. Becker, «On the interactions of the induced flow field of radiators with axial fans», *Experimental Thermal and Fluid Science*, vol. 139, p. 110697, nov. **2022**, doi: 10.1016/j.expthermflusci.2022.110697.

[4] A. Zarri, M. B. Botana, J. Christophe, e C. Schram, «Aerodynamic investigation of the turbulent flow past a louvered-fin-and-tube automotive radiator», *Experimental Thermal and Fluid Science*, vol. 155, p. 111182, giu. **2024**, doi: 10.1016/j.expthermflusci.2024.111182.

[5] P. F. Zhang, M. T. Zhu, Z. J. Li, e K. Wang, «The Cooling Module Aerodynamic Noise Prediction Considering Porous Media», *AMM*, vol. 711, pp. 20–26, dic. **2014**, doi: 10.4028/www.scientific.net/AMM.711.20.

[6] S. Tebib *et al.*, «Detailed noise analysis of automotive engine cooling modules using the Lattice-Boltzmann Method», in *AIAA AVIATION 2023 Forum*, San Diego, CA and Online: American Institute of Aeronautics and Astronautics, giu. **2023**. doi: 10.2514/6.2023-3205.

[7] F. Bellelli, R. Arina, e F. Avallone, «On the impact of operating condition and testing environment on the noise sources in an industrial engine cooling fan», *Applied Acoustics*, vol. 227, p. 110252, gen. **2025**, doi: 10.1016/j.apacoust.2024.110252.

[8] M. Piellard, B. B. Coutty, V. Le Goff, V. Vidal, e F. Perot, «Direct aeroacoustics simulation of automotive engine cooling fan system: effect of upstream geometry on broadband noise», in *20th AIAA/CEAS Aeroacoustics Conference*, Atlanta, GA: American Institute of Aeronautics and Astronautics, giu. **2014**. doi: 10.2514/6.2014-2455.

[9] P. Welch, «The use of fast Fourier transform for the estimation of power spectra: A method based on time averaging over short, modified periodograms», *IEEE Trans. Audio Electroacoust.*, vol. 15, fasc. 2, pp. 70–73, giu. **1967**, doi: 10.1109/TAU.1967.1161901.

[10] L. F. Richardson, «The approximate arithmetical solution by finite differences of physical problems involving differential equations, with an application to the stresses in a masonry dam», *Phil. Trans. R. Soc. Lond. A*, vol. 210, fasc. 459–470, pp. 307–357, gen. **1911**, doi: 10.1098/rsta.1911.0009.

[11] F. Avallone, W. C. P. Van Der Velden, D. Ragni, e D. Casalino, «Noise reduction mechanisms of sawtooth and combed-sawtooth trailing-edge serrations», *J. Fluid Mech.*, vol. 848, pp. 560–591, ago. **2018**, doi: 10.1017/jfm.2018.377.

[12] S. Moreau e M. Sanjose, «Sub-harmonic broadband humps and tip noise in low-speed ring fans», *The Journal of the Acoustical Society of America*, vol. 139, fasc. 1, pp. 118–127, gen. **2016**, doi: 10.1121/1.4939493.

[13] D. Lallier-Daniels, S. Moreau, e M. Sanjose, «Aeroacoustics of a Low-Speed Free Tip Fan With a Complex Clearance Geometry», in *Volume 13: Vibration, Acoustics and Wave Propagation*, Montreal, Quebec, Canada: American Society of Mechanical Engineers, nov. **2014**, p. V013T16A004. doi: 10.1115/IMECE2014-39160.

[14] M. Sturm, M. Sanjosé, S. Moreau, e T. Carolus, «Aeroacoustic simulation of an axial fan including the full test rig by using the lattice boltzmann method», **2015**.

[15] S. Moreau, O. Marck, e M. Roger, «Aero-acoustic installation effects in cooling fan systems PART 2: near-field and ground effects», **2008**.